Ultrasound in Med. & Biol., Vol. 33, No. 6, pp. 870–879, 2007

0301-5629/07/$–see front matter

ELSEVIER

doi:10.1016/j.ultrasmedbio.2006.10.016

● *Original Contribution*

MORPHOLOGICAL AND FUNCTIONAL EVALUATION OF MURINE HETEROTOPIC CARDIAC GRAFTS USING ULTRASOUND BIOMICROSCOPY

YU-QING ZHOU,* RAMI BISHAY,† AKIVA FEINTUCH,* KESHENG TAO,† FRASER GOLDING,‡ WEI ZHU,§ LORI J. WEST,† and R. MARK HENKELMAN*¶

*Mouse Imaging Centre, †Department of Infection, Immunity, Injury and Repair, ‡Department of Pediatrics and §Cardiovascular Research Program, The Hospital for Sick Children and ¶Department of Medical Biophysics, University of Toronto, Toronto, Ontario, Canada

(*Received* 12 *June* 2006; *revised* 21 *October* 2006; *in final form* 26 *October* 2006)

Abstract—This study investigated the use of an ultrasound biomicroscope (UBM) to observe murine heterotopic cardiac transplants. By using an UBM (30 MHz), cardiac isografts in eight mice were studied on days 1, 5, 14 and 50 posttransplantation. The same method was tested in allografts in two mice on days 1, 5, 7 and 9. Two-dimensional imaging delineated the graft structures with high spatial resolution. In isografts, M-mode recording showed gradually decreased left ventricular (LV) wall thickness and chamber dimension, but increased LV fractional shortening. Doppler sampling measured blood velocities from the ascending aorta, left coronary artery (LCA), aortic and mitral orifices of grafts. In isografts, LCA forward flow caused by native circulation to perfuse the graft myocardium increased from day 1 to 5, then moderately decreased by day 14 and stabilized thereafter. In allografts, LCA forward flow sharply decreased to almost zero between day 5–9. Therefore, UBM is a reliable method for following the survival status of cardiac grafts in mice. (E-mail: yqzhou@phenogenomics.ca)

Key Words: **Mice, Cardiac transplant, High frequency ultrasound, Doppler.**

INTRODUCTION

The murine heterotopic heart transplantation model, which was first introduced by Corry et al. (1973), has recently become very popular for studying transplant rejection. In this model, the cardiac graft is implanted in the abdomen of a recipient mouse, with the blood flow of the native circulation going through the graft myocardium. The cardiac graft does not work as a pump and the native heart is still needed for maintaining the circulation of the recipient. Because many genetically well-characterized inbred mouse strains are available, and also new transgenic and gene knockout mice have been generated using advanced techniques, heart transplant models in mice with specific genetic disparities provide powerful tools for elucidating the molecular processes underlying graft rejection (Krieger and Fathman 1997; Haber and Shi 1997; Koglin and Russell 1999; Raisanen-Sokolowski et al. 1999), for exploring genetic and molecular approaches designed to improve grafts acceptance (Mottram et al. 1998; West and Tao 2002) and for testing antirejection strategies (Kirkman et al. 1985; Mottram et al. 1987).

Several approaches can be used to evaluate the survival or detect the rejection of cardiac grafts in mice. Direct palpation to grade beating strength is a traditional means of monitoring rejection (Corry et al. 1973). However, this method is qualitative and subjective, with large interobserver variability. Endomyocardial biopsy remains the "gold standard" for assessing rejection in humans (Caves et al. 1973) and large animals (Billingham et al. 1973), but it is too destructive for mice. The surface ECG of a heterotopic graft provides valuable information, but its waveforms can be affected by location of electrodes, arbitrary and flexible orientation of the graft (Mottram et al. 1988) and interference from surrounding structures.

L. J. West and K. Tao are now at the Department of Pediatrics and Surgery, Heart Transplantation Research, Faculty of Medicine and Dentistry, 1-130A, Dentistry-Pharmacy Centre, Edmonton, Alberta, Canada T6G 2N8.

Address correspondence to: Yu-Qing Zhou, PhD, Mouse Imaging Centre, The Hospital for Sick Children, 555 University Avenue, Toronto, Ontario, Canada M5G 1X8. E-mail: yqzhou@phenogenomics.ca

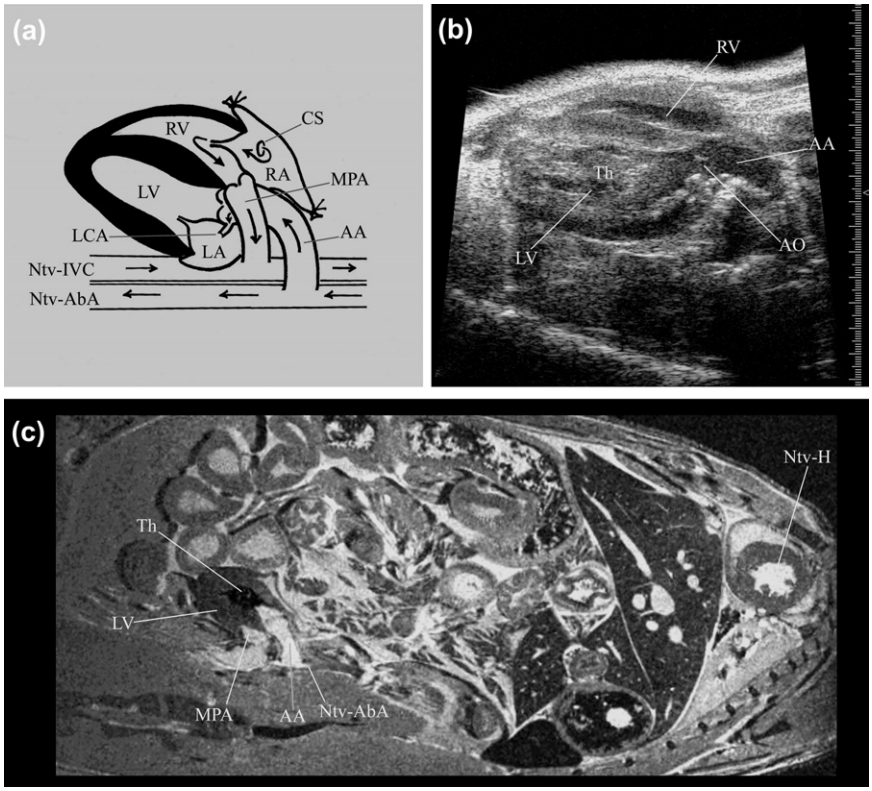

Fig. 1. Illustration of a heterotopic cardiac transplant in mice with typical ultrasound and magnetic resonance imaging (MRI) results. (a) Schematic showing a cardiac graft implanted in a mouse abdomen with ascending aorta (AA) connected to native abdominal aorta (Ntv-AbA) and main pulmonary artery (MPA) connected to native inferior vena cava (Ntv-IVC). The pulmonary veins and venae cavae of the graft are ligated. The intracardiac flow pattern is illustrated. (b) Typical UBM image of an isograft on day 1 posttransplantation, showing the longitudinal section of the flow channel from the aortic anastomosis, AA to the left ventricle (LV). (c) MRI image of a fixed mouse with an isograft on day 50 posttransplantation, showing the native heart (Ntv-H) and the cardiac graft in an oblique sagittal section. AO: aortic orifice; CS: coronary sinus; LCA: left coronary artery; RA: right atrium; RV: right ventricle; Th: thrombus.

Echocardiography using clinical systems has been used to observe the ventricular wall thickness of murine heterotopic cardiac graft (Scherrer-Crosbie et al. 2002), but the limited spatial resolution at clinical frequencies (8 to 12 MHz) seems to preclude its use for a more comprehensive evaluation. Recently, high frequency (20 to 55 MHz) ultrasound biomicroscopy (UBM) has been successfully used for *in vivo* observation of cardiac morphology, function and hemodynamics with much higher spatial resolution (Zhou et al. 2004b; Zhou et al. 2005). Therefore, it is of interest to evaluate murine heterotopic cardiac transplants using this new imaging modality.

The purposes of this study were (1) to establish a method for *in vivo* observation of the morphology and function of heterotopic cardiac grafts in mice using high frequency ultrasound imaging and (2) to delineate the physiology of heterotopic cardiac isografts and its change over time to provide baseline data for future studies of cardiac allografts in mice.

MATERIALS AND METHODS

Mice

Eight C3H/He mice (four males and four females; six to eight weeks old at surgery) were transplanted with syngeneic cardiac grafts (C3H/He) heterotopically placed in the abdomen. The donor mice were of similar age, gender-matched and had similar body weights as the recipients. The procedure of transplantation was originally reported by Corry et al. (1973) and modified in our laboratory (West and Tao 2002). In brief, the donor ascending aorta was anastomosed end-to-side to the recipient abdominal aorta and the donor pulmonary artery trunk to the inferior vena cava (Fig. 1a). After surgery, isografts were monitored by palpation of heart pulsation in awake mice. A qualitative score was assigned from 4 (strongest) to 0 (absence of pulsation) to evaluate graft function according to previously reported criteria (Corry et al. 1973).

Cardiac isografts were observed on days 1, 5, 14

and 50 posttransplantation for structure, function and hemodynamics using UBM. The observation on day 1 (24 h posttransplantation) served to evaluate the functional status of isografts during immediate postoperation recovery. On day 5, grafts were assumed to be completely recovered from surgery. In addition, day 5 corresponds to the onset of acute rejection for allografts (Mottram et al. 1988). Although isografts survive indefinitely, this study on isografts was designed to provide reference data for future studies on allografts. Previous studies on rats showed that the nonworking state of heterotopic cardiac isografts resulted in decreased cardiac weight during the first two weeks posttransplantation, followed by stabilization of cardiac weight afterwards (Klein et al. 1990). Thus, two weeks posttransplantation is an approximate dividing point between acute and long-term changes for isografts. Finally, the observation on day 50 provides a view of the long-term status of the isografts. Native hearts were not observed using UBM.

To explore the potential of UBM imaging to detect acute graft rejection, the left coronary arterial flow pattern of the allografts (BALB/c to C3H/He) in two mice was observed on days 1, 5, 7 and 9 posttransplantation. The surgical and UBM imaging procedures were the same as for the isografts. The survival status of the allografts was also graded by palpation.

The experimental protocol for this study was approved by the Animal Care Committee of the Hospital for Sick Children in Toronto and the study was conducted in accordance with the guidelines established by the Canadian Council on Animal Care.

In vivo imaging of cardiac grafts using UBM

Instrumental specifications. An UBM (Vevo 660, VisualSonics Inc., Toronto, Canada) was used. It has a single element mechanical transducer with a center frequency of 30 MHz and a frame rate of 30Hz. The spatial resolution of 2-D (B-mode) imaging was ~115 μm (lateral) by ~55 μm (axial). Other technical specifications related to M-mode and Doppler function modalities have been described in detail previously (Zhou et al. 2004b; Zhou et al. 2005).

Preparation of animals. Mice were anesthetized using inhaled isoflurane at 1.5% and positioned supine with four paws taped to electrodes on a platform for recording ECG waves which showed the signals from both the native and transplanted hearts. In two mice with isografts, needle electrodes were placed subcutaneously in close proximity to the graft located in the abdomen. This ECG, representing the electric activity of the isograft, was recorded (Mottram et al. 1988) and displayed with the Doppler spectrum for identifying the flow waveforms produced by the graft and for differentiating them from those caused by the native heart. Mouse abdominal hair was cleanly removed using hair-removal cream. Prewarmed ultrasound gel was place on the abdomen for coupling the transducer and tissue. The mouse body temperature was monitored by a rectal thermometer and maintained between 36°C and 38°C.

In vivo UBM imaging. The orientation of cardiac graft was judged by palpation and the graft was usually found to be situated in the right-middle portion of the abdomen, with the cardiac base at midline and the apex pointing inferiorly and to the right. The UBM transducer was first oriented to obtain a longitudinal section of the graft, showing the flow channel from its anastomosis with the native abdominal aorta, retrograde through the ascending aorta and aortic orifice, to the left ventricular outflow tract (Fig. 1b). The Doppler sample volume was placed at the middle portion of the ascending aorta to record a flow velocity spectrum (Fig. 2b and c). Then, the sample volume was moved to the aortic orifice, slightly on the ventricular side, to record the aortic regurgitant jet.

From the above position, the imaging plane was slightly adjusted to visualize the proximal part of the left coronary artery and the Doppler sample volume was placed at a location distal to the origin of the left coronary artery (0.5–1.0 mm away) for recording a flow spectrum (Fig. 3a, b and Fig. 4).

The imaging section was then reoriented to make the longitudinal axis of the left ventricle perpendicular to the ultrasound beam direction in B-mode imaging. M-mode recording was made with a cursor line placed across the largest ventricular chamber dimension.

The transducer was relocated at the graft apex with the central axis of the transducer pointing superiorly, posteriorly and leftwards. In that section, both left ventricular inflow and outflow tracts were viewed. The Doppler sample volume was placed in the mitral orifice, slightly on the ventricular side for left ventricular inflow spectrum during diastole and on the atrial side for mitral regurgitation during systole. By slightly rotating the transducer counterclockwise, the tricuspid orifice was also visualized and the right ventricular diastolic inflow Doppler spectrum was recorded.

Finally, a short axis section of the graft was obtained to visualize the right ventricular outflow tract and the main pulmonary artery. The Doppler pulmonary arterial flow spectrum was recorded at the middle point between the pulmonary orifice and the anastomosis of the main pulmonary artery with the native inferior vena cava.

In all Doppler recordings, the smallest intercept angle between the ultrasound beam and the longitudinal

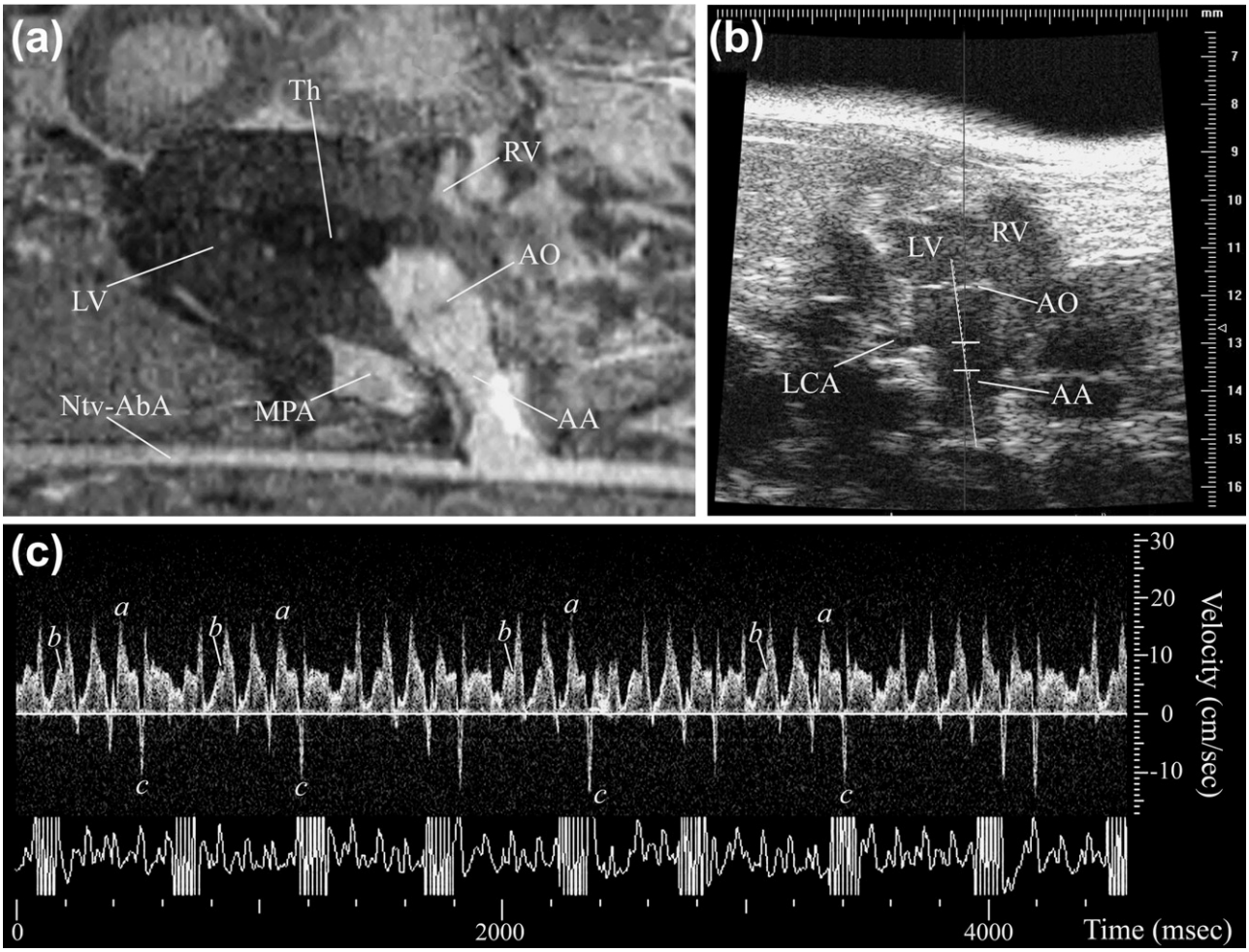

Fig. 2. Flow pattern in the ascending aorta (AA) of a cardiac isograft. (a) MRI image of fixed mouse, showing cardiac isograft and the anastomosis between graft AA and native abdominal aorta (Ntv-AbA). (b) UBM image on day 50 posttransplantation showing a longitudinal section of the flow channel from the aortic anastomosis to the left ventricle (LV), which corresponds to that shown in (a), with Doppler sample volume located in the middle part of AA. (c) Doppler flow spectrum from the AA. The positive waveforms represent the forward flow mainly caused by the pressure of the native circulation perfusing the cardiac isograft and the negative waveforms represent the backward flow produced by the contraction of the isograft. The periodic variation pattern of waveforms is caused by the asynchrony between the native heart and the isograft and is not related to the respiration cycle as manifested by the artificial marks on ECG trace (which was produced by touching the ECG electrode at the end of each inspiration). Several velocities in Doppler waveforms are noted: letter a indicates the peak velocity of the maximal forward waveforms (forward V_{max}), letter b indicates the velocity of forward waveforms at end-diastole (forward Ved), and letter c indicates the peak velocity of the maximal backward waveforms (backward V_{max}). See previous figure legends for the definitions of other abbreviations.

axis of the flow channel was achieved by carefully adjusting the orientations of the transducer and the mouse. The ECG was always recorded simultaneously with the Doppler flow spectrum for data analysis. A complete examination lasted about 30 to 45 min for each mouse.

UBM data analysis

All UBM measurements were made according to the standards established in human echocardiography (Quinones et al. 2002; Sahn et al. 1978). M-mode recording of the left ventricle was analyzed for wall thicknesses, chamber dimensions and fractional shortening.

Because native and transplanted hearts beat at different rates, the interaction between the native circulation and the graft yielded complicated flow velocity waveforms. Nevertheless, periodically repeated patterns were recognizable in the ascending aorta (Fig. 2c) and in the left coronary artery of grafts (Fig. 3 and Fig. 4). To understand the complex Doppler flow waveforms in left coronary artery, a representative recording from an

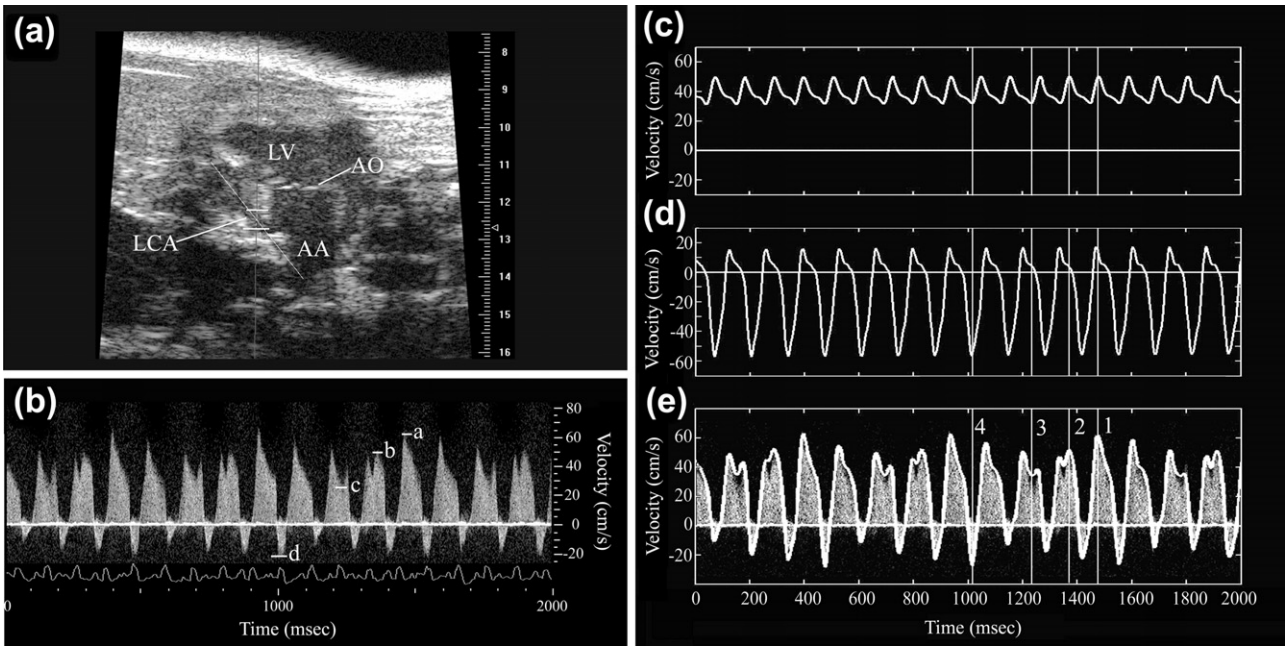

Fig. 3. Flow pattern in left coronary artery (LCA) of an isograft and the method of analysis. (a) UBM image of LCA on day 50 postimplantation, showing the location of the Doppler sample volume. (b) Typical Doppler flow spectrum of the LCA with periodic variation of waveforms caused by asynchrony between the native heart and the isograft. To interpret the data, the waveform was decomposed into two periodic waveforms, as shown in panels (c) and (d) using numerical fitting. (c) The waveform representing the forward flow perfusing the myocardium of the graft, which is assumed to be caused by native circulation alone. (d) The waveform assumed to be produced solely by the activity of the cardiac isograft, with forward (positive) flow during ventricular relaxation and backward (negative) flow during ventricular contraction of the isograft. (e) The summed waveform of panels (c) and (d), which closely represents the real Doppler waveform shown in panel (b). In panels (c) to (e), line 1 marks the peak systole of the native heart and the maximal diastole of the graft, producing the maximal forward flow velocity (forward V_{max}) as indicated by letter a in panel (b). Line 2 is at the peak systole of the native heart when the flow velocity caused by the graft is close to zero, resulting in moderate forward flow velocity as indicated by letter b in panel (b). Line 3 is at the end diastole of the native heart when the flow velocity produced by the graft is close to zero, yielding the notch with minimal forward velocity (forward Ved) as indicated by letter c in panel (b). Line 4 is at the maximal contraction of the graft against the lowest forward flow at the end-diastole of the native circulation, producing the maximal backward velocity (backward V_{max}) as indicated by letter d in panel (b). See previous figure legends for the definitions of other abbreviations.

isograft was mathematically analyzed (Fig. 3). The Doppler signal was assumed to be the sum of two periodic waveforms with different frequencies corresponding to the beating rates of native and transplanted hearts. The velocity waveform for each heart was represented by a sum of sinusoids with arbitrary amplitude and phase of the corresponding frequency and its first, second and third harmonics. The amplitudes and phases were then extracted by numerically fitting the sum of those two waveforms to the actual Doppler spectrum recording. The resulting two periodic waveforms represent the flow caused by the native circulation (Fig. 3c) and by the isograft (Fig. 3d). Matlab (The MathWorks, Inc., Natick, MA, USA) was used for numerical fitting. As demonstrated, the flow waveform in the left coronary artery caused by native circulation is similar to a peripheral arterial flow pattern. The relaxation of the isograft during diastole yields an additional forward flow in left coronary artery. Conversely, the contraction of the graft produces a backward flow, most probably by squeezing the coronary vasculature.

Based on the analysis above, the forward waveforms of highest amplitude appeared when the native heart contracted and the graft simultaneously relaxed. The maximal velocity was the sum of the peak velocity caused by the systolic pressure of the native circulation and the forward flow velocity caused by graft relaxation and measured as the forward V_{max}. The composite waveforms with notches on the top represented the turning point from end-diastole to start of systole of the native heart. The peaks of moderate amplitude following notches occurred when the flow caused by the graft is close to zero and represented the real peak systolic velocity caused by the native circulation. However, this peak was not always identifiable. The lowest points of the notches represented the real end-diastolic velocity

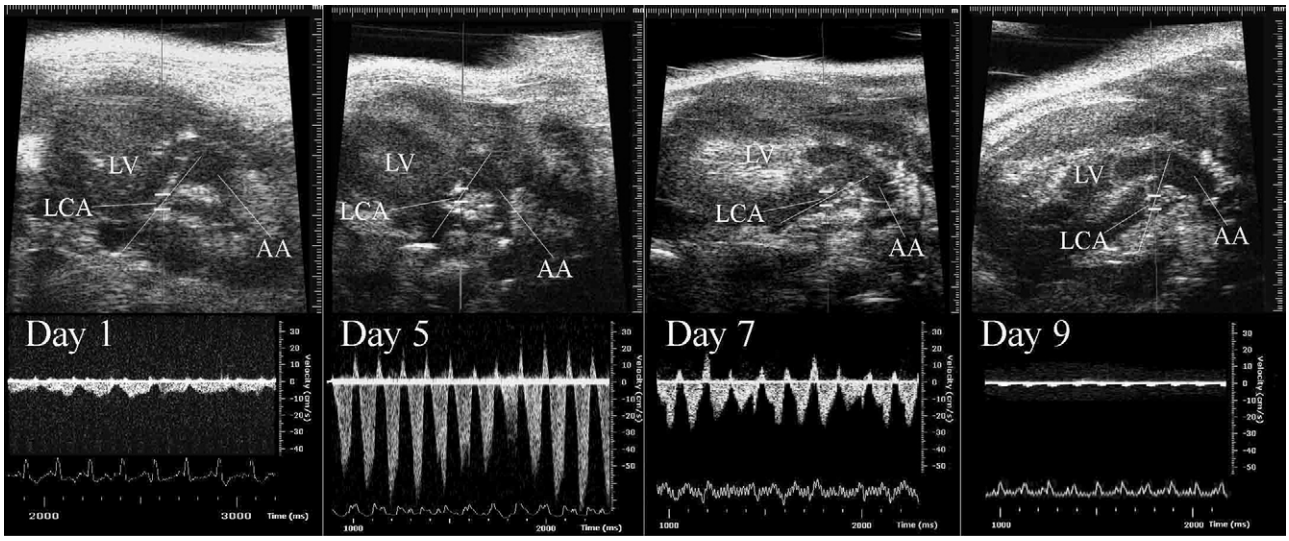

Fig. 4. Doppler flow spectra of the left coronary artery (LCA) in an allograft on day 1, day 5, day 7 and day 9 posttransplantation. Note the modified imaging orientation and the consequent direction of the Doppler flow waveforms compared to Fig. 3. See previous figure legends for the definitions of other abbreviations.

(forward Ved) produced by the native heart because it occurred when the flow caused by the graft is close to zero (Fig. 3b to e). The backward waveform of highest amplitude occurred when the graft contracted and the native heart relaxed and so the maximal velocity represents the peak velocity caused by the contraction of the graft against the end-diastolic pressure in the native circulation and measured as the backward V_{max} (Fig. 3b–e). The time-velocity integral was also measured for the highest forward and backward Doppler flow waveforms. When both heart rates were close to each other, similar waveforms as seen in the cases with more different heart rates were still recordable, but with a longer cycle time of the periodical interference pattern. In that situation, a bigger time window was used to record Doppler flow spectrum from more cardiac cycles.

The flow spectrum in the isograft aorta was analyzed and quantified in a similar way as described above (Fig. 2c). In analyzing aortic and mitral regurgitations, the peak velocities of some regurgitant jets were higher than the upper limit of the UBM system and, therefore, just semiquantitatively evaluated as higher or lower than 200 cm/s. For the main pulmonary artery, the peak-velocity and time-velocity integral of forward flow waveforms were also measured. Because the mitral and tricuspid inflow waveforms were small in amplitude and variable in pattern, they were not quantified.

All Doppler parameters were averaged for three cardiac cycles. The native heart rate was measured from the forward waveforms of the aortic Doppler recording. The graft heart rates were measured from the backward waveforms of the aortic flow and left coronary flow and the forward flow waveform of the main pulmonary artery and averaged.

Anatomical confirmation of cardiac grafts by magnetic resonance imaging (MRI)

After UBM examination on day 50, two mice were perfused with gadopentetate dimeglumine (Magnevist®, Berlex Canada Inc., Quebec, Canada) and fixed by infusing formalin for MRI (Johnson et al. 2002; Zhou et al. 2004a) using a 7-T magnet (Magnex Scientific, Oxford, UK) controlled by a Varian spectrometer (Palo Alto, CA, USA), as previously described (Bock et al. 2003). We used a conventional spin-echo pulse sequence with the following imaging parameters: 600 ms repetition time, 18 ms echo time, 60 mm × 28 mm × 28 mm field of view, and 600 × 280 × 280 imaging matrix providing isotropic voxels of 100 μm resolution. The three-dimensional MRI data were visualized and analyzed with Amira software (TGS Inc., San Diego, CA, USA) for comparative assignments of the cardiac structures visualized by UBM imaging in similar sections (Zhou et al. 2004b).

Statistics

Changes of measured parameters over the observation period were analyzed using one-way repeated measures analysis of variance (ANOVA). The Student-Newman-Keuls method was used for all pairwise multiple comparisons (SigmaStat, Statistical Solutions). All data are expressed as mean ± standard

Table 1. The morphological and functional measurements of cardiac isografts in seven mice using *in vivo* UBM imaging on days 1, 5, 14 and 50 posttransplantation (mean ± SEM)

Parameter	Day 1	Day 5	Day 14	Day 50
Body weight (g)	22 ± 1	23 ± 1	24 ± 1[a,b]	28 ± 1[a,b,c]
Native heart rate (bpm)	480 ± 9	505 ± 25	529 ± 7	496 ± 13
Graft heart rate (bpm)	404 ± 19	494 ± 21[a]	484 ± 28[a]	479 ± 16[a]
Ascending aorta				
Forward V_{max} (cm/s)	15.1 ± 1.8	17.0 ± 2.0	14.9 ± 2.2	15.4 ± 1.7
Forward Ved (cm/s)	2.4 ± 0.4	5.0 ± 0.4[a]	3.2 ± 0.7	6.2 ± 1.2[a,c]
Forward TVI (cm)	0.6 ± 0.1	0.8 ± 0.1	0.6 ± 0.1	0.8 ± 0.1
Backward V_{max} (cm/s)	14.4 ± 3.2	10.7 ± 1.3	11.7 ± 3.0	28.1 ± 5.7[a,b,c]
Backward TVI (cm)	0.3 ± 0.1	0.2 ± 0.1	0.2 ± 0.1	0.5 ± 0.1[a,b,c]
Left coronary artery				
Forward V_{max} (cm/s)	18.1 ± 2.2	51.1 ± 7.5[a]	25.1 ± 3.8[b]	36.6 ± 7.0
Forward Ved (cm/s)	10.2 ± 1.4	29.5 ± 3.8[a]	12.0 ± 2.0[b]	18.4 ± 3.5[b]
Forward TVI (cm)	1.5 ± 0.2	3.1 ± 0.3[a]	1.7 ± 0.3[b]	2.2 ± 0.4
Backward V_{max} (cm/s)	6.2 ± 1.3	21.2 ± 1.9[a]	7.9 ± 2.8[b]	12.2 ± 2.6[b]
Backward TVI (cm)	0.2 ± 0.1	0.5 ± 0.1[a]	0.2 ± 0.1[b]	0.3 ± 0.1[b]
Left ventricle / M-mode				
AWed (mm)	1.1 ± 0.1	1.2 ± 0.1	1.1 ± 0.1	1.0 ± 0.1
EDD (mm)	2.8 ± 0.1	2.4 ± 0.1[a]	1.9 ± 0.1[a,b]	1.9 ± 0.1[a,b]
PWed (mm)	1.1 ± 0.1	1.1 ± 0.1	1.0 ± 0.1	0.8 ± 0.1[a,b]
AWes (mm)	1.1 ± 0.1	1.2 ± 0.1	1.1 ± 0.1	1.0 ± 0.1
ESD (mm)	2.7 ± 0.1	2.2 ± 0.1[a]	1.7 ± 0.1[a,b]	1.5 ± 0.1[a,b]
PWes (mm)	1.1 ± 0.1	1.1 ± 0.1	1.0 ± 0.1	0.9 ± 0.1[a,b]
FS (%)	4.0 ± 1.6	6.9 ± 4.2	9.6 ± 2.4	19.2 ± 5.0[a,b,c]
Main pulmonary artery				
V_{max} (cm/s)	13.7 ± 3.0	72.9 ± 13.2[a]	50.2 ± 9.1[a]	44.7 ± 4.3[a]
TVI (cm)	0.5 ± 0.1	3.2 ± 0.6[a]	1.9 ± 0.5[b]	1.7 ± 0.3[b]

V_{max}: maximal velocity at peak systole; Ved: velocity at end of diastole; TVI: time-velocity integral; AWed: left ventricular anterior wall thickness at end-diastole; EDD: left ventricular end-diastolic diameter; PWed: left ventricular posterior wall thickness at end-diastole; AWes: left ventricular anterior wall thickness at end-systole; ESD: left ventricular end-systolic diameter; PWes: left ventricular posterior wall thickness at end-systole; FS: fractional shortening.

The letters [a], [b], [c] represent significant difference ($p < 0.05$) compared with the corresponding parameter on day 1, 5 and 14 posttransplantation, respectively.

error of the mean (SEM) and statistical significance was set at $p < 0.05$.

RESULTS

One mouse with an isograft was excluded from the statistical analysis because of the reopening of the foramen ovale on the atrial septum (confirmed in UBM imaging) after day 14 posttransplantation. In the remaining seven mice, there was no significant difference in heart rate between the native heart and the cardiac isograft, except that the isograft heart rates on day 1 were lower than those observed later (Table 1). On day 50 posttransplantation, the palpation grading of all isograft was 4 except for the excluded mouse, where it was 3.

As visualized by B-mode imaging, fresh thrombus filled almost the whole left ventricle during the early posttransplantation period (days 1 to 5) and presented as homogeneously hypoechogenic (relative to the moderately echogenic myocardium) and nearly static content. In contrast, a small amount of moving blood flow was seen as moving speckles around the aortic and mitral orifices. The left atrial chamber was not observable (Fig. 1b). From day 14 to 50 posttransplantation, the thrombus in left ventricle became smaller in size and inhomogeneously hyperechogenic. In the left ventricular chamber, a larger free space with moving blood flow was observed, along with a significantly dilated left atrium. Old thrombus in the left ventricle was confirmed by dissection in all mice at the end of the study.

In the ascending aorta of the isografts, the maximal velocity of forward flow toward the graft did not change significantly throughout the observed period, but the end-diastolic velocity showed inconsistent fluctuations. Higher end-diastolic velocities corresponded temporarily to the increase in coronary flow on day 5 and the increase of the flow through the left heart on day 50 posttransplantation, as indicated below. Considering the backward flow produced by the contraction of the isograft against the pressure of the native circulation, the maximal velocity did not change before day 14, but increased significantly thereafter (Table 1). Aortic regurgitant jets were detected at all observed time points and in all seven mice with isografts. The amplitude of the regurgitant jet varied widely during the early posttransplantation period,

but was consistently higher (five of seven > 200 cm/s) on day 50.

In the left coronary artery, the maximal velocity and end-diastolic velocity of forward flow to perfuse the myocardium of the isograft significantly increased from day 1 to 5, then moderately decreased from day 5 to 14 and remained consistent thereafter. The maximal velocity of backward flow produced by the contraction of the isograft showed a similar trend (Table 1).

Mitral regurgitation was detectable in most mice, but was absent in one mouse on day 1, in two mice on day 5 and in one mouse on day 14. The amplitude of the mitral regurgitant jet consistently increased from day 1 (all seven mice < 200 cm/s) to day 14 (five of seven mice > 200 cm/s) and stabilized thereafter.

As Table 1 shows, the left ventricular anterior wall thickness was consistent throughout the posttransplantation period, but the posterior wall thickness gradually decreased and the left ventricular chamber dimension was reduced. In contrast, the left ventricular fractional shortening increased with time, significantly from day 14 to 50.

The peak-velocity and time-velocity integral of the main pulmonary artery significantly increased from day 1 to 5, then decreased from day 5 to 14 and stayed consistent thereafter (Table 1). This temporal pattern is similar to that of the left coronary arterial flow, possibly due to the fact that all blood flow in the right heart comes from the coronary vasculature in this model.

MRI in two fixed mice clearly demonstrated the connections between the cardiac graft and the native vessels, the overall morphology of the graft and its detailed internal structures such as the thrombus. By manipulating the plane in the three-dimensional data set, the sections corresponding to *in vivo* UBM imaging views were carefully analyzed for comparative assignments of the cardiac structures, as shown in Fig. 1 and Fig. 2.

In the two mice with allografts, the palpation grading of the grafts was 4 on day 1, 3 on day 5, 2 on day 7 and 1 on day 9 posttransplantation. The Doppler flow spectra of the left coronary artery showed that both forward flow to perfuse the graft myocardium and backward flow caused by graft contraction sharply decreased after day 5 to 7 to almost zero on day 9 (Fig. 4 and Fig. 5).

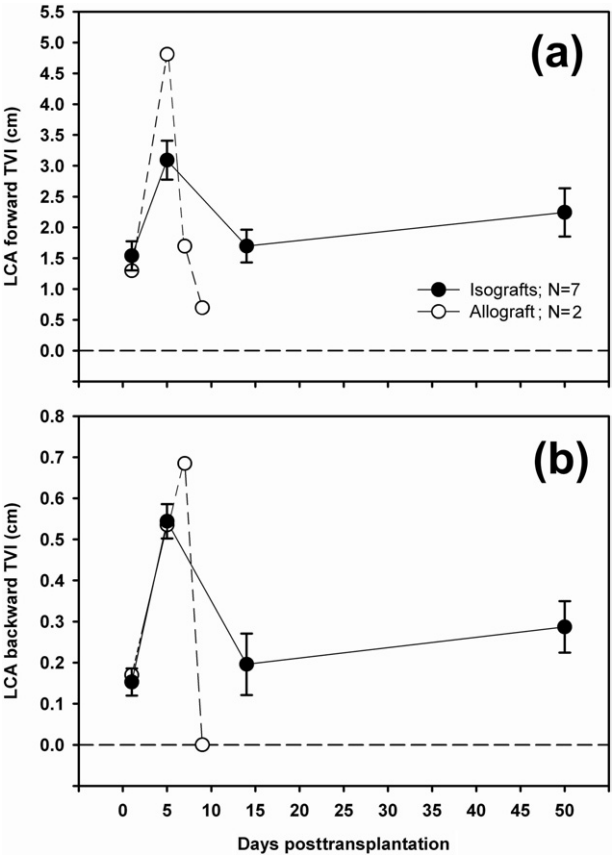

Fig. 5. Temporal changes of averaged Doppler flow parameters in the left coronary artery (LCA) of two allografts in contrast with those of seven isografts. (a) The time-velocity integral of the maximal forward waveforms (forward TVI). (b) The time-velocity integral of the maximal backward waveforms (backward TVI).

DISCUSSION

This study shows the ability of high frequency ultrasound imaging to characterize heterotopic cardiac transplants in mice noninvasively and comprehensively. Two-dimensional imaging visualizes with high spatial resolution the overall morphology and intracardiac structures. Left ventricular dimensions and fractional shortening can be evaluated using M-mode recording. By using Doppler, flow-velocity patterns are readily estimated at the ascending aorta, aortic orifice, left coronary artery, mitral and tricuspid orifices and the main pulmonary artery. Longitudinal changes in morphology, function and flow dynamics of cardiac grafts can be followed throughout the posttransplantation period.

Coronary arterial flow is directly relevant to the myocardial blood perfusion of grafts and, therefore, is a major focus of this study. Any pathologic changes in myocardium and capillary would first affect the coronary vascular resistance and, consequently, the coronary arterial flow measurement. Concerning the changes of global and regional myocardial blood flow related to graft rejection, previous studies on canine models have yielded conflicting results (Saloman et al. 1977; Bando et al. 1991; Pirolo et al. 1993). However, most studies on rat heterotopic heart transplants found clear evidence of significant decrease in myocardial blood flow in associ-

ation with histologically confirmed rejection (Hamano et al. 1989; Bergsland et al. 1989; Szabo et al. 2001). Szabo et al. (2001) observed in rat isografts that myocardial blood flow completely recovered within the first day postoperatively and remained stable afterwards to day 5. In allografts, a significant fall in myocardial blood flow was detected three days after transplantation, corresponding to mild or moderate rejection confirmed by histology (Szabo et al. 2001). Our data from mouse isografts during the early posttransplantation period are generally in agreement with the above findings in rats, although the recovery of coronary flow in mouse isografts was slightly delayed. In our mouse model, the decrease in forward coronary flow from day 5 to 14 and the stabilization thereafter were most probably attributable to long-term changes of the myocardium and the coronary vasculature of grafts. Histologic observation of rat isografts three weeks posttransplantation revealed graft atrophy associated with a disappearance of capillaries, possibly reflecting decreased needs for nutrients and oxygen transport in the "nonworking" grafts (Rakusan et al. 1997). Backward flow showed a similar temporal pattern as forward flow, suggesting that greater myocardial perfusion results in better ventricular contraction. In the present study, the left coronary arterial flow parameters in those two rejecting allografts indicates the rapid decrease of flow perfusion to the graft myocardium and the consequent decrease of graft contractility after day 5 posttransplantation. The different temporal patterns of coronary flow between isografts and allografts suggest their potential for predicting acute rejection.

The left ventricular wall thickness of isografts increased on day 1 to 5 posttransplantation, compared with previous measurements of donor hearts before transplantation (~0.73 mm in C57BL/6 mice) (Scherrer-Crosbie et al. 2002). The increased ventricular wall thickness during the early posttransplantation period is attributable to ischemic damage and reperfusion injury, including cellular swelling, increased vascular permeability and consequent interstitial edema (Scherrer-Crosbie et al. 2002; Worrall et al. 1996; Rabkin et al. 1999). In addition, under-filling of the left ventricular cavity in this heterotopic cardiac transplantation model reduced chamber dimensions and artificially increased the wall thickness (Scherrer-Crosbie et al. 2002). However, the long-term decrease in the left ventricular wall thickness of isografts is attributable to the ventricular atrophy due to decreased hemodynamic load in the left ventricle, as suggested in previous studies on rat heterotopic isografts (Klein et al. 1990; Rakusan et al. 1997).

The reduced ventricular chamber dimension of grafts relative to that of native hearts (end-diastolic dimension was ~4 mm for C57BL/6 mice of similar age and body weight) (Zhou et al. 2004b; Zhou et al. 2005) and its further decrease throughout the posttransplantation period may be caused by under-filling and absence of physiological pressure in the left ventricle. As found in rats, artificially created aortic regurgitation by puncturing the aortic valves before graft implantation, in an attempt to increase hemodynamic load to the left ventricle of isografts, can significantly increase left ventricular chamber dimension, maintain left ventricular compliance and partially preserve ventricular mass relative to the isografts without aortic regurgitation (Spencer et al. 2003).

In contrast, left ventricular fractional shortening significantly increased with time. Postischemic depression of ventricular function should be a major reason for the low left ventricular fractional shortening during early days posttransplantation. The thrombus in the left ventricular chamber might also affect left ventricular contraction. The left ventricular chamber was largest in the early days, but most of the chamber was occupied by fresh thrombus. This may partially explain why the left ventricular fractional shortening did not increase significantly on day 5, when the best blood perfusion to the coronary system occurred. With advancing time, the thrombus got smaller in size and, consequently, more free space in left ventricle for moving blood became available and more significant ventricular volume change became possible. The consistently high aortic and mitral regurgitations, the increased backward flow in the ascending aorta and the dilated left atrium during the late period of observation all suggested the movement of a larger amount of blood flow through the left heart and, consequently, a larger change of left ventricular volume throughout the cardiac cycle. On the other hand, the aortic and mitral regurgitations were due to the absence of normal pressure gradients across valvular orifices for properly closing valves in this "non-physiological" condition. The interaction between two asynchronous hearts also contributes to the valvular regurgitation.

SUMMARY

This study demonstrates the feasibility of using high frequency ultrasound imaging comprehensively to evaluate heterotopic cardiac grafts in mice. The morphology, function and flow dynamics of grafts can be followed in a serial manner using B-mode imaging, M-mode recording and Doppler flow-velocity sampling. Specific temporal patterns have been found for coronary blood perfusion, left ventricular dimensions and function of isografts. The preliminary data from the rejecting allografts suggest the potential of Dopp-

ler coronary flow parameters for predicting acute rejection.

Acknowledgments—Sources of funding: this work is part of the Mouse Imaging Centre (MICe) at the Hospital for Sick Children and the University of Toronto. The infrastructure was funded by the Canada Foundation for Innovation (CFI) and Ontario Innovation Trust (OIT). The research was funded by an Ontario Research and Development Challenge Fund (ORDCF) grant to the Ontario Consortium for Small Animal Imaging (OCSAI) and also the Heart and Stroke Foundation of Ontario. RMH and LJW hold a Canada Research Chair. YQZ consults to VisualSonics Inc., Toronto. The authors thank Lynda Cockroft for the help in manuscript preparation.

REFERENCES

Bando K, Fraser CD Jr., Chacko VP, Pillai R, Jacobus WE, Cameron DE, Hutchins GM, Reitz BA, Baumgartner WA. Coronary blood flow does not decrease during allograft rejection in heterotopic heart transplants. J Heart Lung Transplant 1991;10(2):251–256.

Bergsland J, Hwang K, Driscoll R, Carr EA, Wright JR, Curran-Everett DC, Carroll M, Krasney E, Krasney JA. Coronary blood flow and thallium 201 uptake in rejecting rat heart transplantations. J Heart Transplant 1989;8(2):147–153.

Billingham ME, Caves PK, Dong E Jr., Shumway NE. The diagnosis of canine orthotopic cardiac allograft rejection by transvenous endomyocardial biopsy. Transplant Proc 1973;5(1):741–743.

Bock NA, Konyer NB, Henkelman RM. Multiple-mouse MRI. Magn Reson Med 2003;49:158–167.

Caves PK, Stinson EB, Billingham ME, Rider AK, Shumway NE. Diagnosis of human cardiac allograft rejection by serial cardiac biopsy. J Thorac Cardiovasc Surg 1973;66(3):461–466.

Corry RJ, Winn HJ, Russell PS. Heart transplantation in congenic strains of mice. Transplant Proc 1973;5(1):733–735.

Haber E, Shi C. The role of specific genes in transplant arteriosclerosis: Studies in mutant mice. Transpl Immunol 1997;5(4):293–297.

Hamano K, Ohmi M, Esato K, Mohri H. Myocardial tissue blood flow in allotransplanted rat heart with a special reference to acute rejection. J Heart Transplant 1989;8(1):48–52.

Johnson GA, Cofer GP, Gewalt SL, Hedlund LW. Morphologic phenotyping with MR microscopy: The visible mouse. Radiology 2002;222:789–793.

Kirkman RL, Barrett LV, Gaulton GN, Kelley VE, Ythier A, Strom TB. Administration of an anti-interleukin 2 receptor monoclonal antibody prolongs cardiac allograft survival in mice. J Exp Med 1985;162(1):358–362.

Klein I, Hong C, Schreiber SS. Cardiac atrophy in the heterotopically transplanted rat heart: *In vitro* protein synthesis. J Mol Cell Cardiol 1990;22(4):461–468.

Koglin J, Russell ME. Alloimmune-mediated apoptosis: comparison in mouse models of acute and chronic cardiac rejection. Transplantation 1999;67(6):904–909.

Krieger NR, Fathman CG. The use of CD4 and CD8 knockout mice to study the role of T-cell subsets in allotransplant rejection. J Heart Lung Transplant 1997;16(3):263–267.

Mottram PL, Wheelahan J, Mirisklavos A, Clunie GJ, McKenzie IF. Prolongation of murine cardiac allografts following treatment of graft recipients with monoclonal anti-L3T4 and Ly-2 antibodies. Transplant Proc 1987;19(1 Pt 1):582–585.

Mottram PL, Smith JA, Mason A, Mirisklavos A, Dumble LJ, Clunie GJ. Electrocardiographic monitoring of cardiac transplants in mice. Cardiovasc Res 1988;22(5):315–321.

Mottram PL, Raisanen-Sokolowski A, Glysing-Jensen T, Stein-Oakley AN, Russell ME. Redefining peripheral tolerance in the BALB/c to CBA mouse cardiac allograft model: Vascular and cytokine analysis after transient CD4 T cell depletion. Transplantation 1998;66(11):1510–1518.

Pirolo JS, Liptay MJ, Brunt EM, Shuman TA, Cox JL, Ferguson TB Jr. Early cardiac allograft rejection is independent of regional myocardial blood flow. Ann Thorac Surg 1993;55(2):441–449.

Quinones MA, Otto CM, Stoddard M, Waggoner A, Zoghbi WA. Recommendations for quantification of Doppler echocardiography: A report from the Doppler Quantification Task Force of the Nomenclature and Standards Committee of the American Society of Echocardiography. J Am Soc Echocardiogr 2002;15:167–184.

Rabkin DG, Jia CX, Spotnitz HM. Attenuation of reperfusion injury with probucol in the heterotopic rat cardiac isograft. J Heart Lung Transplant 1999;18(8):775–780.

Raisanen-Sokolowski A, Glysing-Jensen T, Russell ME. Donor and recipient contributions of ICAM-1 and P-selectin in parenchymal rejection and graft arteriosclerosis: insights from double knockout mice. J Heart Lung Transplant 1999;18(8):735–743.

Rakusan K, Heron MI, Kolar F, Korecky B. Transplantation-induced atrophy of normal and hypertrophic rat hearts: Effect on cardiac myocytes and capillaries. J Mol Cell Cardiol 1997;29(3):1045–1054.

Sahn DJ, DeMaria A, Kisslo J, Weyman A. Recommendations regarding quantitation in M-mode echocardiography: Results of a survey of echocardiographic methods. Circulation 1978;58:1072–1083.

Salomon NW, Stinson EB, Hanley J, Griepp RB, Shumway NE. Alterations in myocardial blood flow during acute rejection of orthotopic canine cardiac allografts. Surg Forum 1977;28:250–252.

Scherrer-Crosbie M, Glysing-Jensen T, Fry SJ, Vancon AC, Gadiraju S, Picard MH, Russell ME. Echocardiography improves detection of rejection after heterotopic mouse cardiac transplantation. J Am Soc Echocardiogr 2002;15(10 Pt 2):1315–1320.

Spencer AU, Hart JP, Cabreriza SE, Rabkin DG, Weinberg AD, Spotnitz IIM. Aortic regurgitation in the heterotopic rat heart transplant: effect on ventricular remodeling and diastolic function. J Heart Lung Transplant 2003;22(8):937–945.

Szabo G, Batkai S, Dengler TJ, Bahrle S, Stumpf N, Notmeyer W, Zimmermann R, Vahl CF, Hagl S. Systolic and diastolic properties and myocardial blood flow in the heterotopically transplanted rat heart during acute cardiac rejection. World J Surg 2001;25(5):545–552.

West LJ, Tao KS. Acceptance of third-party cardiac but not skin allografts induced by neonatal exposure to semi-allogeneic lymphohematopoietic cells. Am J Transplant 2002;2:733–744.

Worrall NK, Chang K, Suau GM, Allison WS, Misko TP, Sullivan PM, Tilton RG, Williamson JR, Ferguson TB Jr. Inhibition of inducible nitric oxide synthase prevents myocardial and systemic vascular barrier dysfunction during early cardiac allograft rejection. Circ Res 1996;78(5):769–779.

Zhou YQ, Davidson L, Henkelman RM, Nieman BJ, Foster FS, Yu LX, Chen XJ. Ultrasound-guided left ventricular catheterization: A novel method of whole mouse perfusion for microimaging. Lab Invest 2004a;84:385–389.

Zhou YQ, Foster FS, Nieman BJ, Davidson L, Chen XJ, Henkelman RM. Comprehensive transthoracic cardiac imaging in mice using ultrasound biomicroscopy with anatomical confirmation by magnetic resonance imaging. Physiol Genomics 2004b;18:232–244.

Zhou YQ, Zhu Y, Bishop J, Davidson L, Henkelman RM, Bruneau BG, Foster FS. Abnormal cardiac inflow patterns during postnatal development in a mouse model of Holt-Oram syndrome. Am J Physiol Heart Circ Physiol 2005;289(3):H992–H1001.